



**HAL**  
open science

# Diffusion Models for Counterfactual Explanations

Guillaume Jeanneret, Loïc Simon, Frédéric Jurie

► **To cite this version:**

Guillaume Jeanneret, Loïc Simon, Frédéric Jurie. Diffusion Models for Counterfactual Explanations. 16th Asian Conference on Computer Vision (ACCV2022), Dec 2022, Macao, China. 10.1007/978-3-031-26293-7\_14 . hal-04583065

**HAL Id: hal-04583065**

**<https://hal.science/hal-04583065>**

Submitted on 27 May 2024

**HAL** is a multi-disciplinary open access archive for the deposit and dissemination of scientific research documents, whether they are published or not. The documents may come from teaching and research institutions in France or abroad, or from public or private research centers.

L'archive ouverte pluridisciplinaire **HAL**, est destinée au dépôt et à la diffusion de documents scientifiques de niveau recherche, publiés ou non, émanant des établissements d'enseignement et de recherche français ou étrangers, des laboratoires publics ou privés.

# Diffusion Models for Counterfactual Explanations

Guillaume Jeanneret, Loïc Simon, and Frédéric Jurie

Normandy University, ENSICAEN, UNICAEN, CNRS, GREYC, France  
guillaume.jeanneret-sanmiguel@unicaen.fr

**Abstract.** Counterfactual explanations have shown promising results as a post-hoc framework to make image classifiers more explainable. In this paper, we propose DiME, a method allowing the generation of counterfactual images using the recent diffusion models. By leveraging the guided generative diffusion process, our proposed methodology shows how to use the gradients of the target classifier to generate counterfactual explanations of input instances. Further, we analyze current approaches to evaluate spurious correlations and extend the evaluation measurements by proposing a new metric: Correlation Difference. Our experimental validations show that the proposed algorithm surpasses previous state-of-the-art results on 5 out of 6 metrics on CelebA.

## 1 Introduction

Convolutional neural networks (CNNs) reached performances unimaginable a few decades ago, thanks to the adoption of very large and deep models with hundreds of layers and nearly billions of trainable parameters. Yet, it is difficult to explain their decisions because they are highly non-linear and over-parametrized. Moreover, for real-life applications, if a model exploits spurious correlations of data to forecast a prediction, the end-user will doubt the validity of the decision. Particularly, in high-stake scenarios like medicine or critical systems, ML must guarantee the usage of correct features to compute a prediction and prevent counterfeit associations. For this reason, the Explainable Artificial Intelligence (XAI) research field has been growing in recent years to progress towards understanding the decision-making mechanisms in black-box models.

In this paper, we focus on post-hoc explanation methods. Notably, we concentrate on the growing branch of Counterfactual Explanations (CE) [63]. CE aim to create minimal but meaningful perturbations of an input sample to change the original decision given by a fixed pretrained model. Although the objective between CE and adversarial examples share some similarities [44], the CE' perturbations must be understandable and plausible. In contrast, adversarial examples [37] contain high-frequency noise *indistinguishable* to the human eye. Overall, CE target four goals: *(i)* the explanations must flip the input's forecast using *(ii)* sparse modifications, *i.e.* instances with the smallest perturbation. Additionally, *(iii)* the explanations must be realistic and understandable by a

human. Lastly, *(iv)* the counterfactual generation method must create diverse instances. In general, counterfactual explanations seek to reveal the learned correlations related to the model’s decisions.

Multiple works on CE use generative models to create tangible changes in the image [27, 48, 51]. Further, these architectures recognize the factors to generate images near the image-manifold [4]. Given the recent advances within image synthesis community, we propose DiME: Diffusion Models for counterfactual Explanations. DiME harnesses the denoising diffusion probabilistic models [19] to produce CE. For simplicity, we will refer to these models as diffusion models or DDPMs. To the best of our knowledge, we are the first to exploit these new synthesis methods in the context of CE.

Diffusion models offer several advantages compared to alternate generative models, such as GANs. First of all, DDPMs have several latent spaces; each one controls coarse and fine-grained details. We take advantage of low-level noise latent spaces to generate semantically-meaningfully changes in the input image. These spaces only have been recently studied by [38] for inpainting. Secondly, due to their probabilistic nature, they produce diverse sets of images. Stochasticity is ideal for CE because multiple explanations may explain a classifier’s error modes. Third, Nichol and Dhariwal [42] results suggest that DDPMs cover a broader range of the target image distribution. Indeed, they noticed that for similar FID, the recall is much higher on the improved precision-recall metrics [32]. Finally, DDPMs’ training is more stable than the state-of-the-art synthesis models, notably GANs. Due to their relatively new development, DDPMs are under-studied, and multiple aspects are yet to be deciphered.

We contribute a small step into the XAI community by studying the low-level noised latent spaces of DDPMs in the context of counterfactual explanations. We summarize our contributions on three axes:

- **Methodology:** (i) DiME uses the recent diffusion models to generate counterfactual examples. Our algorithm relies on a single unconditional DDPM to achieve instance counterfactual generation. To accomplish this, (ii) we derive a new way to leverage an existing (target) classifier to guide the generation process instead of using one trained on noisy instances, such as in [11]. Additionally, (iii) to reduce the computational burden, we take advantage of the forward and backward diffusion chains to transfer the gradients of the classifier under observation.
- **Evaluation:** We show that the standard MNAC metric is misleading because it does not account for possible spurious correlations. Consequently, we introduce a new metric, dubbed Correlation Difference, to evaluate subtle spurious correlations on a CE setting.
- **Performance:** We set a new state-of-the-art result on CelebA, surpassing the previous works on CE on the FID, FVA, and MNAC metrics for the *Smile* attribute and the FID and MNAC for the *Young* feature.

To further boost research on counterfactual explanations, our code and models are publicly available on Github.

## 2 Related Work

Our work contributes to the field of XAI, within which two families can be distinguished: *interpretable-by-design* and *post-hoc* approaches. The former includes, at the design stage, human interpretable mechanisms [2, 3, 6, 9, 22, 40, 71]. The latter aims at understanding the behavior of existing ML models without modifying their internal structure. Our method belongs in this second family. The two have different objectives and advantages; one benefit of *post-hoc* methods is that they rely on existing models that are known to have good performance, whereas XAI by design often leads to a performance trade-off.

**Post-hoc methods:** In the field of *post-hoc* methods, there are several explored directions. Model Distillation strategies [13, 58] approach explainability through fitting an interpretable model on the black-box models’ predictions. In a different vein, some methods generate explanation in textual form [17, 43, 68]. When it comes to explaining visual information, feature importance is arguably the most common approach, often implemented in the form of saliency maps computed either using the gradients within the network [8, 26, 33, 53, 64, 74] or using the perturbations on the image [45, 46, 62, 70]. Concept attribution methods seek the most recurrent traits that describe a particular class or instance. Intuitively, concept attribution algorithms use [29] or search [13, 14, 69, 75] for human-interpretable notions such as textures or shapes.

**Counterfactual Explanations (CE):** CE is a branch of *post-hoc* explanations. They are relevant to legally justify decisions made automatically by algorithms [63]. In a nutshell, a CE is the smallest meaningful change to an input sample to obtain a desirable outcome of the algorithm. Some recent methods [15, 65] exploit the query image’s regions and a different classified picture to interchange semantic appearances, creating counterfactual examples. Despite using the same terminology, this line of work [15, 61, 66] is diverging towards a task where it merely highlights regions that explains the discrepancy of the decision between the two real images, significantly differing from our evaluation protocol setup. Other works [52, 63] leverage the input image’s gradients with respect to the target label to create meaningful perturbations. Conversely, [1] find patterns via prototypes that the image must contain to alter its prediction. Similarly, [36, 47] follow a prototype-based algorithm to generate the explanations. Even Deep Image Priors [59] and Invertible CNNs [23] have shown the capacity to produce counterfactual examples. Furthermore, theoretical analyses [24] found similarities between counterfactual explanations and adversarial attacks.

Due to the nature of the problem, the generation technique used is the key element to produce data near the image manifold. For instance, [12] optimizes the residual of the image directly using an autoencoder as a regularizer. Other works propose to use generative networks to create the CE, either unconditional [27, 41, 48, 54, 73] or conditional [34, 55, 60]. In this paper, we adopt more recent generation approaches, namely diffusion models; an attempt never considered in the past for counterfactual generation.

**Diffusion Models:** Diffusion models have recently gained popularity in the image generation research field [19, 56]. For instance, DDPMs approached in-

painting [49], conditional and unconditional image synthesis [10, 19, 42], super-resolution [50], even fundamental tasks such as segmentation [5], providing performance similar or even better than State-of-the-Art generative models. Further, studies like [20, 57] show score-based approaches and diffusion are alternative formulations to denoise the reverse sampling for data generation. Due to the recursive generation process, DDPMs sampling is expensive. Many works have studied alternative approaches to accelerate the generation process [31, 67].

The recent method of [11] targets conditional image generation with diffusion models, which they do by training a specific classifier on noisy instances to bias the generation process. Our work bears some similarities to this method, but, in our case, explaining an existing classifier trained uniquely in clean instances poses additional challenges. In addition, unlike past diffusion methods, we perform the image editing process from an intermediate step rather than the final one. To the best of our knowledge, no former study has considered diffusion models to explain a neural network counterfactually.

### 3 Methodology

#### 3.1 Diffusion Model Preliminaries

We begin by introducing the generation process of diffusion models. They rely on two Markov chain sampling schemes that are inverse of one another. In the forward direction, the sampling starts from a natural image  $x$  and iteratively sample  $z_1, \dots, z_T$  by replacing part of the signal with white Gaussian noise. More precisely, letting  $\beta_t$  be a prescribed variance, the forward process follows the recursive expression:

$$z_t \sim \mathcal{N}(\sqrt{1 - \beta_t} z_{t-1}, \beta_t I), \quad (1)$$

where  $\mathcal{N}$  is the normal distribution,  $I$  the identity matrix, and  $z_0 = x$ . In fact, this process can be simulated directly from the original sample with

$$z_t \sim \mathcal{N}(\sqrt{\alpha_t} x, (1 - \alpha_t) I), \quad (2)$$

where  $\alpha_t := \prod_{k=1}^t (1 - \beta_k)$ . For clarification, through the rest of the paper, we will refer to clean images with an  $x$ , while noisy ones with a  $z$ .

In the reverse process, a neural network recurrently denoises  $z_T$  to recover the previous samples  $z_{T-1}, \dots, z_0$ . This network takes the current time step  $t$  and a noisy sample  $z_t$  as inputs, and produces an average sample  $\mu(t, z_t)$  and a covariance matrix  $\Sigma(t, z_t)$ , shorthanded as  $\mu(z_t)$  and  $\Sigma(z_t)$ , respectively. Then  $z_{t-1}$  is sampled with

$$z_{t-1} \sim \mathcal{N}(\mu(z_t), \Sigma(z_t)). \quad (3)$$

So, the DDPM algorithm iteratively employs Eq. 3 to generate an image  $z_0$  with zero variance, *i.e.* a clean image. Some diffusion models use external information, such as labels, to condition the denoising process. However, in this paper, we employ an unconditional DDPM.

In practice, the variances  $\beta_t$  in Eq. 1 are chosen such that  $z_T \sim \mathcal{N}(0, I)$ . Further, the DDPM’s trainable parameters are fitted so that the reverse and forward processes share the same distribution. For a thorough understanding on the DDPM training, we recommend the studies of Ho *et al.* [19] and Nichol and Dhariwal [42] to the reader. Once the network is trained, one can rely on the reverse Markov chain process to generate a clean image from a random noise image  $z_T$ . Besides, the sampling procedure can be adapted to optimize some properties following the so-called guided diffusion scheme proposed in [11]<sup>1</sup>:

$$z_{t-1} \sim \mathcal{N}(\mu(z_t) - \Sigma(z_t) \nabla_{z_t} L(z_t; y), \Sigma(z_t)), \quad (4)$$

where  $L$  is a loss function using  $z_t$  to specify the wanted property of the generated image, for example, to condition the generation on a prescribed label  $y$ .

### 3.2 DiME: Diffusion Models for Counterfactual Explanations

We take an image editing standpoint on CE generation, as illustrated Fig. 1. We start from a query image  $x$ . Initially, we rely on the forward process starting from  $x_\tau = x$  to compute a noisy version  $z_\tau$ , with  $1 \leq \tau \leq T$ . Then we go back in the reverse Markov chain using the guided diffusion (Eq 4) to recover a counterfactual (hence altered) version of the query sample. Building upon previous approaches for CE based on other generative models [25, 55, 63], we rely on a loss function composed of two components to steer the diffusion process: a classification loss  $L_{class}$ , and a perceptual loss  $L_{perc}$ . The former guides the image edition into imposing the target label, and the latter drives the optimization in terms of proximity.

In the original implementation of the guided diffusion [11], the loss function uses a classifier applied directly to the current noisy image  $z_t$ . In their context, this approach is appropriate since the considered classifier can make robust predictions under noisy observations, *i.e.* it was trained on noisy images. Regardless, such an assumption on the classifier under scrutiny would imply a substantial limitation in the context of counterfactual examples. We circumvent this obstacle by adapting the guided diffusion mechanism. To simplify the notations, let  $x_t$  be the clean image produced by the iterative unconditional generation on Eq 3 using as the initial condition  $z_t$ . In fact, this makes  $x_t$  a *function* of  $z_t$  because we denoise  $z_t$  recursively with the diffusion model  $t$  times to obtain  $x_t$ . Luckily, we can safely apply the classifier to  $x_t$  since it is not noisy. So, we express our loss as:

$$L(z_t; y, x) = \mathbb{E} [\lambda_c L_{class}(C(y|x_t)) + \lambda_p L_{perc}(x_t, x)] := \mathbb{E} [\tilde{L}(x_t; y, x)], \quad (5)$$

where  $C(y|x_t)$  is the posterior probability of the category  $y$  given  $x_t$ , and  $\lambda_c$  and  $\lambda_p$  are constants. Note that an expectation is present due to the stochastic nature of  $x_t$ . In practice, computing the loss gradient would require sampling several

<sup>1</sup> In [11], the guided diffusion is restricted to a specific classification loss. Still, for the sake of generality and conciseness, we provide its extension to an arbitrary loss.

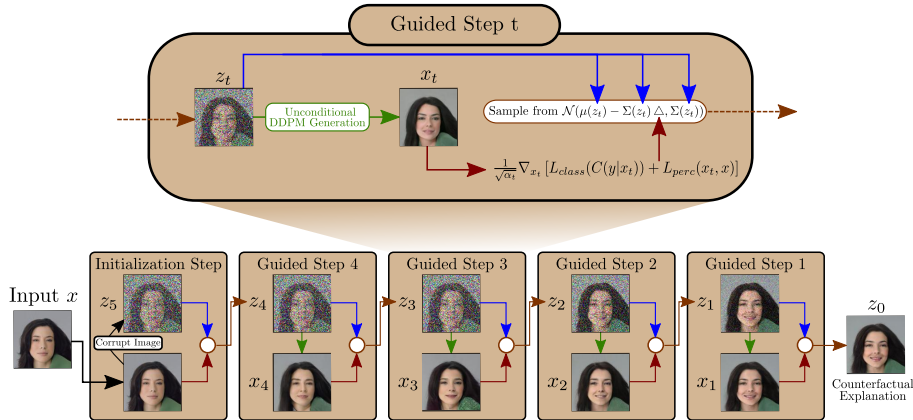


**Fig. 1. DiME: Diffusion Models for Counterfactual Explanations.** Given an input instance  $x$ , we perturb it following Eq. 2 to get  $z_\tau$  (here  $\tau = 5$ ). At time step  $t$ , we use the DDPM model to generate a clean image  $x_t$  to obtain the clean gradient  $L_{class}$  and  $L_{perc}$  with respect to  $x_t$ . Finally, we sample  $z_{t-1}$  using the guiding optimization process on Eq. 4, using the previously extracted clean gradients.

realizations of  $x_t$  and taking an empirical average. We restrict ourselves to a single realization per step  $t$  for computational reasons and argue that this is not an issue. Indeed, we can partly count on an averaging effect along the time steps to cope with the lack of individual empirical averaging. Besides, the stochastic nature of our implementation is, in fact, an advantage because it introduces more diversity in the produced CE, a desirable feature as advocated by [48].

Using this strategy, the dependence of the loss on  $x_t$ , rather than directly from  $z_t$ , renders the gradient computation more challenging. Indeed, formally it would require to apply back-propagation from  $x_t$  back to  $z_t$ :

$$\nabla_{z_t} L(z_t; y, x) = \left( \frac{Dx_t}{Dz_t} \right)^T \cdot \nabla_{x_t} \tilde{L}(x_t; y, x). \quad (6)$$

Unfortunately, this computation requires retaining Jacobian information across the entire computation graph, which is very deep when  $t$  is close to  $\tau$ . As a result, backpropagation is too memory intensive to be considered an option. To bypass this pitfall, we shall rely on the forward sampling process, which operates in a single stage (Eq. 2). Using the re-parametrization trick [30], one obtains

$$z_t = \sqrt{\alpha_t} x_t + \sqrt{1 - \alpha_t} \epsilon, \quad \epsilon \sim \mathcal{N}(0, \mathbf{I}). \quad (7)$$

Thus, by solving  $x_t$  from  $z_t$ , we can leverage the gradients of the loss function with respect to the noisy input, a consequence of the chain rule. Henceforth, the gradients of  $L$  with respect to the noisy image become

$$\nabla_{z_t} L(z_t; y, x) = \frac{1}{\sqrt{\alpha_t}} \nabla_{x_t} \tilde{L}(x_t; y, x). \quad (8)$$

This approximation is possible since the DDPM estimates the reverse Markov chain to fit the forward corruption process. Thereby, both processes are similar.

To sum up, Fig. 1 depicts the generation of a counterfactual explanation with our algorithm: DiME. We start by corrupting the input instance  $x = x_\tau$  following Eq. 2 up to the noise level  $t = \tau$ . Then, we iterate the following two stages until  $t = 0$ : (i) First, using the gradients of the previous clean instance  $x_{t-1}$ , we guide the diffusion process to obtain  $z_{t-1}$  using Eq. 4 with the gradients computed in Eq. 8. (ii) Next, we estimate the clean image  $x_t$  for the current time step  $z_{t-1}$  with the unconditional generation pipeline of DDPMs. The final instance is the counterfactual explanation. If we do not find an explanation that fools the classifier under observation, we increase the constant  $\lambda_c$  and repeat the process.

**Implementation Details.** In practice, we incorporate additionally an  $\ell_1$  loss,  $\eta\|z_t - x\|_1$ , between the noisy image  $z_t$  and the input  $x$  to improve the  $\ell_1$  metric on the pixel space. We empirically set  $\eta$  small to avoid any significant impact on the quality of the explanations. Our diffusion model generates faces using 500 diffusion steps from the normal distribution. We re-spaced the sampling process to boost inference speed to generate images with 200 time-steps at test time. We use the following hyperparameters settings:  $\lambda_p = 30$ ,  $\eta = 0.05$ , and  $\tau = 60$ . Finally, we set  $\lambda_c \in \{8, 10, 15\}$  to iteratively find the counterfactuals. We consider that our method failed if we do not find any explanation after exhausting the values of  $\lambda_c$ . To train the unconditional DDPM model, we used the publicly available code of [11]. Our model has the same architecture as the ImageNet’s Unconditional DDPM, but we used 500 sampling steps. Furthermore, the inner number of channels was set to 128 instead of 256 given CelebA’s lower complexity. For training, we completed 270,000 iteration with a batch size of 75 with a learning rate of  $1 \times 10^{-4}$  with a weight decay of 0.05.

## 4 Experiments

**Dataset.** In this paper, we study the CelebA dataset [35]. Following standard practices, we preprocess all images to a  $128 \times 128$  resolution. CelebA contains 200k images, labeled with 40 binary attributes. Previous works validate their methods on the smile and young binary attributes, ignoring all other attributes. Finally, the architecture to explain is a DenseNet121 [21] classifier. Given the binary nature of the task, the target label is always the opposite of the prediction. If the model correctly estimates an instance’s label, we flip the model’s forecast. Otherwise, we modify the input image to classify the image correctly.

**Experimental goals.** In this section, we evaluate our CE approach using standard metrics. Also, we develop new tools to go beyond the current evaluation practices. Let us recap the principles of current evaluation metrics, following previous works [48, 55]. The first goal of CE is to create realistic explanations that flip the classifier under observation. The capacity to change the classifier decision is typically exposed as a flip ratio (FR). Following the image synthesis research literature, the Frechet Inception Distance [18] (FID) measures the fidelity of the image distribution. The second goal of CE methods is to create



	Smile			Young		
Method	FID ( $\downarrow$ )	FVA ( $\uparrow$ )	MNAC ( $\downarrow$ )	FID ( $\downarrow$ )	FVA ( $\uparrow$ )	MNAC ( $\downarrow$ )
xGEM+ [27]	66.9	91.2	-	59.5	97.5	6.70
PE [55]	35.8	85.3	-	53.4	72.2	3.74
DiVE [48]	29.4	97.3	-	33.8	<b>98.2</b>	4.58
DiVE <sup>100</sup>	36.8	73.4	4.63	39.9	52.2	4.27
DiME	<b>3.17</b>	<b>98.3</b>	<b>3.72</b>	<b>4.15</b>	95.3	<b>3.13</b>

**Table 1. State-of-the-Art results.** We compare our model performance against the State-of-the-Art on the FID, FVA and MNAC metrics. The values in **bold** are the best results. All metrics were extracted from [48]. Our model has a 10 fold improvement on the FID metric. We extracted all results from Rodriguez *et al.*' work [48].

proximal and sparse images. Among other tools, the XAI community adopted the Face Verification Accuracy [7] (FVA) and Mean Number of Attributes Changed (MNAC) [48]. On the one hand, the MNAC metric looks at the face attributes that changed between the input image and its counterfactual explanation, disregarding if the individual's identity changed. Finally, the FVA looks at the individual's identity without considering the difference of attributes.

As a quick caveat, let us mention that this set of standard metrics displays several pitfalls that we shall address in more detail later. First, these metrics do not evaluate the diversity of the produced explanations, whereas this is an important factor. Besides, some of the metrics are at odds with a crucial purpose of CE, namely the detection of potential spurious correlations.

#### 4.1 Realism, Proximity and Sparsity Evaluation

To begin with, the FVA is the standard metric for face recognition. To measure this value, we used the cosine similarity between the input image and its produced counterfactual on the feature space of a ResNet50 [16] pretrained model on VGGFace2 [7]. This metric considers that two instances share identity if the similarity is higher than 0.5. So, the FVA is the mean number of faces sharing the same identity with their corresponding CE. Secondly, to compute the MNAC, we fine-tuned the VGGFace2 model on the CelebA dataset. We refer to the fine-tuned model as the oracle. Thus, the MNAC is the mean number of attributes for which the oracle switch decision under the action of the CE. For a fair comparison with the state-of-the-art, we trained all classifiers, including the fine-tuned ResNet50 for the MNAC assessment, using the DiVE's [48] available code. Finally, previous studies [48, 55] compute the FID, the FVA, and the MNAC metrics considering only those successful counterfactual examples.

DiVE do not report their flip rate (FR). This raises a concern over the fairness comparing against our method. Since some metrics depend highly on the number of samples, especially FID, we recomputed their CE. To our surprise, their flip ratio was relatively low: 44.6% for the smile category. In contrast, we

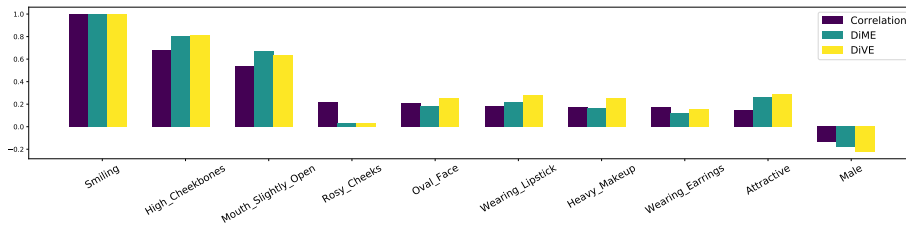


**Fig. 2. Spurious Correlation Detection.** We show the top 9 most correlated attributes in the label space with “smile”. We obtained the Pearson Correlation Coefficient from the ground truth on the training set. Albeit the difference in the MNAC measure, DiME and DiVE achieve to detect the correlations similarly.

achieved a success rate of 97.6 and 98.9 for the smile and young attributes, respectively. Therefore, we calculated the explanations with 100 optimization steps and reported the results as DiVE<sup>100</sup>. The new success rates are 92.0% for smile and 93.4% for young.

We show DiME’s performance in Table 1. Our method beats the previous literature in five out of six metrics. For instance, we have a  $\sim 10$ -fold improvement on the FID metric for the smile category, while the young attribute has an  $\sim 8$  fold improvement. We credit these gains to our generation process since it does not require entirely corrupting the input instance; hence, the coarse details of the image remain. The other methods rely on latent space-based architectures. Thus, they require to compact essential information removing outlier data. Consequently, the generated CE cannot reconstruct the missing information, losing significant visual components of the image statistics.

Despite the previous advantages, we cannot fail to notice that DiME is less effective in targeting the young attribute than the smile. The smile and young attributes have distinct features. The former is delineated by localized regions, while the latter scatters throughout the entire face. Thus, the gradients produced by the classifier differ between the attributes of choice; for the smile attribute, the gradients are centralized while they are outspread for the young attribute. We believe that this subtle difference underpins the slight drop of performance (especially with respect to FVA) in the young attribute case. This hypothetical explanation should be confirmed by a more systematic study of various attributes, though this phenomenon is out of scope of the paper.

## 4.2 Discovering Spurious Correlations

The end goal of CE is to uncover the modes of error of a target model, in particular its reliance on spurious correlations. Current evaluation protocols [55] search to assess the counterfeit dependencies by inducing artificial entanglements between two supposedly uncorrelated traits such as the smile and gender attributes. In our opinion, such an extreme experiment does not shed light on the ability to reveal spurious correlations for two reasons. First, the introduced entanglement

is complete, in the sense that in this experiment the two considered attributes are fully correlated. Second, the entanglement is restricted to two attributes. In fact, as depicted in Fig. 2, in real datasets such as CelebA, many labels are correlated at multiple levels. As a result, this phenomenon calls the previously proposed correlation experiment into question.

At the same time, the interpretation of some standard metric can be challenged when spurious correlations are present. This is the case for MNAC which corresponds to the mean number of attributes that change under the action of a CE method. Arguably, the classical interpretation is that attributes being unrelated, a CE method that change fewer attributes (in addition to the target) is preferable. In other words between two CE methods, the one displaying the smaller MNAC is reckoned as the better one. This interpretation is at odd with the fact that the alternative method may display a higher MNAC because it actually reveals existing spurious correlations.

Consequently, we design a new metric called Correlation Difference (CD), verifying the following principles: (i) it quantifies how well a counterfactual routine captures spurious correlations. In other words, it estimates correlations between two attributes after applying the counterfactual algorithm and compare these estimates to the true dataset correlations. (ii) It should apply an oracle to predict the (unknown) attributes of counterfactual examples. (iii) The metric should preferably rely on attribute prediction changes between the original example and its explanation to mitigate potential errors of the oracle, rather than solely on the prediction made on the counterfactual. Principle (i) actually amends the failure of MNAC, while (ii) and (iii) maintain its desirable features.

To do so, we start from the definition of the Pearson correlation coefficient  $c_{q,a}$  between the target attribute  $q$  and any other attribute  $a$ . Denoting  $X$  a random image sample, along with its two associated binary attribute labels  $Y_q$  and  $Y_a$ , then  $c_{q,a} = \text{PCC}(Y_q, Y_a)$ , where PCC is the Pearson correlation coefficient operator. To cope with principle (i) we would like to estimate correlations between attributes  $q$  and  $a$  and we would like our estimation to rely on the CE method  $M$  targeting the attribute  $q$ . The main issue is that we do not know the actual attributes for the CE,  $M(X, q)$ , obtained from an image  $X$ . Yet, following principle (ii), we may rely on an oracle to predict these attributes. More precisely, letting  $O_a(X)$  be the oracle prediction for a given image  $X$  and for the label  $a$ , we could simply compute the correlation coefficient between  $O_q(M(X, q))$  and  $O_a(M(X, q))$ . Such an estimate would be prone to potential errors of the oracle, and following principle (iii) we would prefer to rely on attribute changes  $\delta_{q,a}^M(X) = O_a(M(X, q)) - O_a(X)$ .

Interestingly,  $c_{q,a}$  can be reformulated as follows:

$$c_{q,a} = \text{PCC}(\delta_q, \delta_a), \quad (9)$$

where  $\delta_a = Y_a - Y'_a$  (resp.  $\delta_q = Y_q - Y'_q$ ), with  $(X, Y_q, Y_a)$  and  $(X', Y'_q, Y'_a)$  two independent samples. In other words,  $c_{q,a}$  can be interpreted as the correlation between changes in attributes  $q$  and  $a$  among random pairs of samples. Accordingly, we use  $\delta_{q,q}^M$  and  $\delta_{q,a}^M$  as drop-in replacements for  $\delta_q$  and  $\delta_a$  in Eq. 9 to

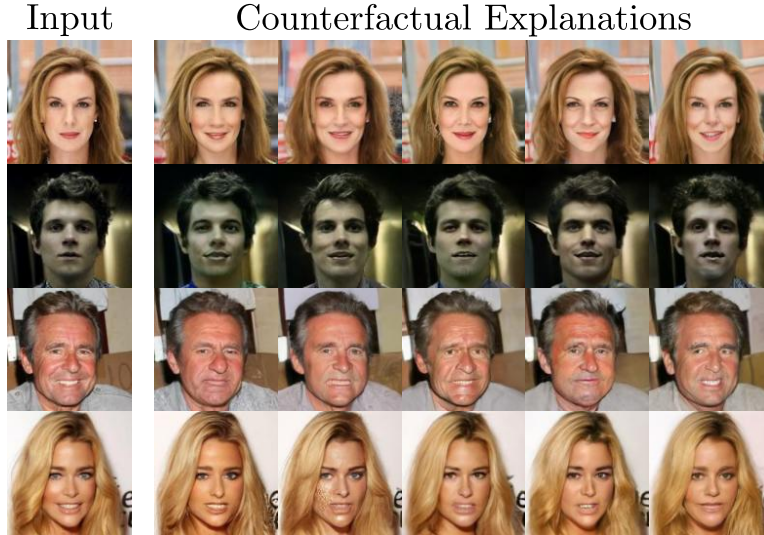


**Fig. 3. Diversity Counterfactual examples.** The classifier predicts first two input images as non-smiley and the last two as smiley. In this example all explanations fool the classifier. Our CE pipeline is capable of synthesising diverse counterfactuals without any additional mechanism.

obtain the estimate  $c_{q,a}^M$  of  $c_{q,a}$  that relies on the label changes produced by the counterfactual method  $M$ . Finally, CD for label  $q$  is merely:

$$CD_q = \sum_a |c_{q,a} - c_{q,a}^M|. \quad (10)$$

We apply our proposed metric on DiME and DiVE<sup>100</sup>'s explanations. We got a CD of 2.30 while DiVE<sup>100</sup> 2.33 on CelebA's validation set, meaning that DiVE<sup>100</sup> lags behind DiME. However, the margin between the two approaches is only slender. This reveals our suspicions: the MNAC results presented in Table 1 give a misleading impression of a robust superiority of DiME over DiVE<sup>100</sup>.

### 4.3 Diversity Assessment

One of the most crucial traits of counterfactual explanations methodologies is the ability to create multiple and diverse examples [39, 48]. As stated in the methodology section, DiME's stochastic properties enable the sampling of diverse counterfactuals. To measure the capabilities of different algorithms to produce multiple explanations, we computed the mean pair-wise LPIPS [72] metric between five independent runs. Formally, setting  $N$  as the length of the dataset and  $n = 5$  as the number of samples, the Diversity metric  $\sigma_L$  is:

$$\sigma_L = \frac{1}{N} \sum_{i=1}^N \frac{2}{n(n+1)} \sum_{j=1}^n \sum_{k=j+1}^n LPIPS(x_j^i, x_k^i), \quad (11)$$

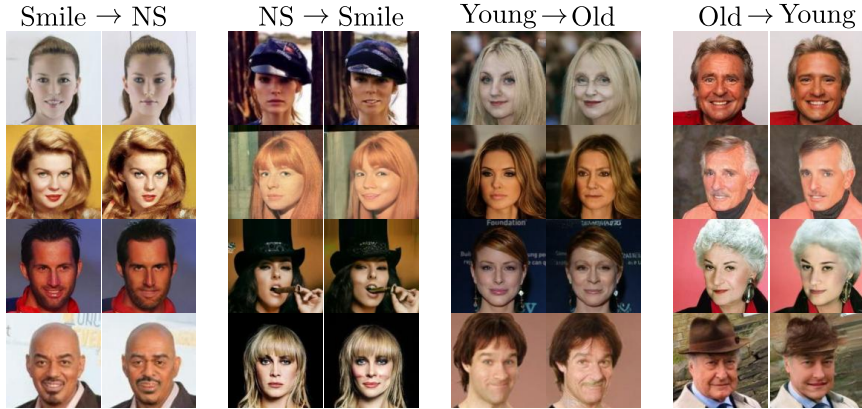


**Fig. 4. Qualitative Results.** We visualize some images and its corresponding counterfactual explanation produced by our proposed approach. Our methodology achieves to incorporate small but perceptually tangible changes in the image. NS stands for Non-Smiley.

A higher  $\sigma_L$  means increased perceptual dissimilarities between the explanations, hence, more diversity. To compute the evaluation metric, we use all counterfactual examples, even the unsuccessful instances, because we search the capacity of exploring different traits. Note that we exclude the input instance to compute the metric since we search for the dissimilarities between the counterfactuals. We compared DiME’s performance with DiVE<sup>100</sup> and its Fisher Spectral variant on a small partition of the validation subset.

We visualize some examples in Fig. 3. All runs achieve similar performances making DiME insensible to the initial random seed. We achieved a  $\sigma_L$  of 0.213. In contrast, DiVE [48] and its Spectral Fisher variant obtained much lower LPIPS diversity of 0.044 and 0.086, respectively. Recall that DiME does not have an explicit mechanism to create diverse counterfactuals. Its only mechanism is the stochasticity within the sampling process (Eqs. 3 and 4). In contrast, DiVE relies on a diversity loss when optimizing the eight explanations. Yet, our methodology achieves higher  $\sigma_L$  metric even without an explicit mechanism.

#### 4.4 Qualitative Results

We visualize some inputs (left) and the counterfactual examples (right) produced by DiME in Fig. 4. We show visualizations for the attributes smile and young. At first glance, the results reveal that the model performs semantical editings into the input image. In addition, uncorrelated features and coarse structure remain almost unaltered. We observe slight variations on some items, such as the pendants, or out-of-distribution shapes such as hands. DiME fails to reconstruct the exact shape of these objects, but the essential aspect remains the same.

Method	FR ( $\uparrow$ )	FID <sup>+</sup> ( $\downarrow$ )	$\ell_1$ ( $\downarrow$ )
Direct	19.7	<b>50.51</b>	0.0454
Naive	70.0	98.93 $\pm$ 2.36	0.0624
Early Stopping	97.3	51.97 $\pm$ 0.77	0.0467
Unconditional <sup>§</sup>	8.6	53.22 $\pm$ 0.98	0.0492
DiME	<b>97.9</b>	<b>50.20</b> $\pm$ 1.00	<b>0.0430</b>

**Table 2. DiME vs variations.** This table shows the advantages of the proposed adjustment to incorporate the classifier under observation. Including the clean gradients benefits DiME on all metrics, especially the FR. <sup>§</sup> FID<sup>+</sup> and  $\ell_1$  are computed with the same number of samples as the rest, but without filtering out unsuccessful CEs.

#### 4.5 Ablation study: Impact of the noise-free input of the classifier

As a major contribution, we have proposed an adjustment over the guided diffusion process. It consists in applying the classifier on noise-free images  $x_t$  rather than on the current noisy version  $z_t$  to obtain a robust gradient direction. One can rightly wonder how important a role is played by this adjustment. To assess this matter, we consider several alternatives to our approach. The first alternative, dubbed Direct, uses the gradient (without the factor  $1/\sqrt{\alpha_t}$ ) of the classifier applied directly to the noisy instance  $z_t$ . The second alternative, called Naive, uses the gradient of the original input image at each time step to guide the optimization process. Therefore, it is not subject to noise issues, but it disregards the guidance that was already applied until time step  $t$ . The last variation is a near duplicate of DiME except for the fact that it ends the guided diffusion process as soon as  $x_t$  fools the classifier. We name this approach Early Stopping. Eventually, we will also evaluate the DDPM generation without any guiding and beginning from the corrupted image at time-step  $\tau$  to mark a reference of the performance of the DDPM model. We will refer to this variant as the Unconditional one.

To validate all distinct variants, we created a small and randomly selected mini-val to evaluate the various metrics. To make FID values more comparable amongst all variants, we condition its computation only on the successful CE and keep the same number of samples for all methods to mitigate the bias in FID with respect to the number of samples. We denote this fair FID as FID<sup>+</sup>. Likewise to the FR and FID<sup>+</sup>, we evaluate the  $\ell_1$  metric on successful CE.

We show the results of the different variations in Table 2. The most striking point is that when compared to the Naive and Direct approaches, the unimpaired version of DiME is the most effective in terms of FR by a large margin. This observation validates the need for our adjustment of the guided diffusion process. Further, our approach is also superior to all other variations in terms of the other metrics. At first glance, we expected the unconditional generation to have better FID than DiME and the ablated methods. However, we believe that the perceptual component of our loss is beneficial in terms of FID. Therefore, the unconditional FID is higher. Based on the same rationale, one can explain

the slightly higher FID displayed by the early stopping variant. Moreover, we noticed that most instances merely shifted the decision boundary, reporting a low confidence of the posterior probability. These instances are semifactual [28] and contain features from both attributes, making them hard to analyze in the context of explainability, in our opinion.

#### 4.6 Limitations

Although we show the benefits of using our model to generate CE, we are far from accomplishing all aspects crucial for the XAI community. For instance, we observe that DiME has two limitations. On the one hand, we adopt the most problematic aspect of DDPMs: the inference time. Namely, DiME uses  $\sim 1800$  times the DDPM model to generate a single explanation. This aspect is undesired whenever the user requires an explanation on the fly. Regardless, DiME can haste its generation process at cost of image quality since diffusion models enjoy from different strategies to boost inference time. On the other hand, we require access to the training data; a limitation shared by many studies. However, this aspect is vital in fields with sensible data. Although access to the data is permitted in many cases, we restrict ourselves to using the data without any labels.

## 5 Conclusion

In this paper, we explore the novel diffusion models in the context of counterfactual explanations. By harnessing the conditional generation of the guided diffusion, we achieve successful counterfactual explanations through DiME. These explanations follow the requirements given by the XAI community: a small but tangible change in the image while remaining realistic. The performance of DiME is confirmed based on a battery of standard metrics. We show that the current approach to validate the sparsity of CE has significant conflicts with the assessment of spurious correlation detection. Our proposed metric, Correlation Difference, correctly measures the impact of measuring the subtle correlation between labels. Further, DiME also exhibits strong diversity in the produced explanation. This is partly inherited from the intrinsic features of diffusion models, but it also results from a careful design of our approach. Finally, we hope that our work opens new ways to compute and evaluate counterfactual explanations.

**Acknowledgements:** Research reported in this publication was supported by the Agence Nationale pour la Recherche (ANR) under award number ANR-19-CHIA-0017.

## References

1. Akula, A., Wang, S., Zhu, S.C.: Cocox: Generating conceptual and counterfactual explanations via fault-lines. *Proceedings of the AAAI Conference on Artificial Intelligence* **34**(03), 2594–2601 (Apr 2020)
2. Alaniz, S., Marcos, D., Schiele, B., Akata, Z.: Learning decision trees recurrently through communication. In: *Proceedings of the IEEE/CVF Conference on Computer Vision and Pattern Recognition (CVPR)*. pp. 13518–13527 (June 2021)
3. Alvarez-Melis, D., Jaakkola, T.S.: Towards robust interpretability with self-explaining neural networks. In: *Advances in neural information processing systems (NeurIPS)* (2018)
4. Arora, S., Risteski, A., Zhang, Y.: Do GANs learn the distribution? some theory and empirics. In: *International Conference on Learning Representations* (2018), <https://openreview.net/forum?id=BJehNfW0>
5. Baranchuk, D., Voynov, A., Rubachev, I., Khruikov, V., Babenko, A.: Label-efficient semantic segmentation with diffusion models. In: *International Conference on Learning Representations* (2022)
6. Bohle, M., Fritz, M., Schiele, B.: Convolutional dynamic alignment networks for interpretable classifications. In: *Proceedings of the IEEE/CVF Conference on Computer Vision and Pattern Recognition (CVPR)*. pp. 10029–10038 (June 2021)
7. Cao, Q., Shen, L., Xie, W., Parkhi, O.M., Zisserman, A.: Vggface2: A dataset for recognising faces across pose and age. In: *2018 13th IEEE International Conference on Automatic Face Gesture Recognition (FG 2018)*. pp. 67–74 (2018). <https://doi.org/10.1109/FG.2018.00020>
8. Chattopadhyay, A., Sarkar, A., Howlader, P., Balasubramanian, V.N.: Grad-cam++: Generalized gradient-based visual explanations for deep convolutional networks. In: *2018 IEEE Winter Conference on Applications of Computer Vision (WACV)*. pp. 839–847 (2018). <https://doi.org/10.1109/WACV.2018.00097>
9. Chen, C., Li, O., Tao, D., Barnett, A., Rudin, C., Su, J.K.: This looks like that: Deep learning for interpretable image recognition. In: Wallach, H., Larochelle, H., Beygelzimer, A., d'Alché-Buc, F., Fox, E., Garnett, R. (eds.) *Advances in Neural Information Processing Systems*. vol. 32. Curran Associates, Inc. (2019)
10. Choi, J., Kim, S., Jeong, Y., Gwon, Y., Yoon, S.: Ilvr: Conditioning method for denoising diffusion probabilistic models. In: *Proceedings of the IEEE/CVF International Conference on Computer Vision (ICCV)*. pp. 14367–14376 (October 2021)
11. Dhariwal, P., Nichol, A.Q.: Diffusion models beat GANs on image synthesis. In: *Thirty-Fifth Conference on Neural Information Processing Systems* (2021)
12. Dhurandhar, A., Chen, P.Y., Luss, R., Tu, C.C., Ting, P., Shanmugam, K., Das, P.: Explanations based on the missing: Towards contrastive explanations with pertinent negatives. In: Bengio, S., Wallach, H., Larochelle, H., Grauman, K., Cesa-Bianchi, N., Garnett, R. (eds.) *Advances in Neural Information Processing Systems*. vol. 31. Curran Associates, Inc. (2018)
13. Ge, Y., Xiao, Y., Xu, Z., Zheng, M., Karanam, S., Chen, T., Itti, L., Wu, Z.: A peek into the reasoning of neural networks: Interpreting with structural visual concepts. In: *Proceedings of the IEEE/CVF Conference on Computer Vision and Pattern Recognition (CVPR)*. pp. 2195–2204 (June 2021)
14. Ghorbani, A., Wexler, J., Zou, J.Y., Kim, B.: Towards automatic concept-based explanations. In: Wallach, H., Larochelle, H., Beygelzimer, A., d'Alché-Buc, F., Fox, E., Garnett, R. (eds.) *Advances in Neural Information Processing Systems*. vol. 32. Curran Associates, Inc. (2019)



15. Goyal, Y., Wu, Z., Ernst, J., Batra, D., Parikh, D., Lee, S.: Counterfactual visual explanations. In: ICML. pp. 2376–2384 (2019)
16. He, K., Zhang, X., Ren, S., Sun, J.: Deep residual learning for image recognition. 2016 IEEE Conference on Computer Vision and Pattern Recognition (CVPR) pp. 770–778 (2016)
17. Hendricks, L.A., Akata, Z., Rohrbach, M., Donahue, J., Schiele, B., Darrell, T.: Generating visual explanations. In: Leibe, B., Matas, J., Sebe, N., Welling, M. (eds.) Computer Vision – ECCV 2016. pp. 3–19. Springer International Publishing (2016)
18. Heusel, M., Ramsauer, H., Unterthiner, T., Nessler, B., Hochreiter, S.: Gans trained by a two time-scale update rule converge to a local nash equilibrium. In: Guyon, I., Luxburg, U.V., Bengio, S., Wallach, H., Fergus, R., Vishwanathan, S., Garnett, R. (eds.) Advances in Neural Information Processing Systems. vol. 30. Curran Associates, Inc. (2017), <https://proceedings.neurips.cc/paper/2017/file/8a1d694707eb0fefe65871369074926d-Paper.pdf>
19. Ho, J., Jain, A., Abbeel, P.: Denoising diffusion probabilistic models. In: Larochelle, H., Ranzato, M., Hadsell, R., Balcan, M.F., Lin, H. (eds.) Advances in Neural Information Processing Systems. vol. 33, pp. 6840–6851. Curran Associates, Inc. (2020)
20. Huang, C.W., Lim, J.H., Courville, A.: A variational perspective on diffusion-based generative models and score matching. In: ICML Workshop on Invertible Neural Networks, Normalizing Flows, and Explicit Likelihood Models (2021)
21. Huang, G., Liu, Z., van der Maaten, L., Weinberger, K.Q.: Densely connected convolutional networks. In: Proceedings of the IEEE Conference on Computer Vision and Pattern Recognition (CVPR) (July 2017)
22. Huang, Z., Li, Y.: Interpretable and accurate fine-grained recognition via region grouping. In: Proceedings of the IEEE/CVF Conference on Computer Vision and Pattern Recognition (CVPR) (June 2020)
23. Hvilshøj, F., Iosifidis, A., Assent, I.: Ecinn: efficient counterfactuals from invertible neural networks. British Machine Vision Conference 2018, BMVC 2021 (2021)
24. Ignatiev, A., Narodytska, N., Marques-Silva, J.: On relating explanations and adversarial examples. In: Wallach, H., Larochelle, H., Beygelzimer, A., d'Alché-Buc, F., Fox, E., Garnett, R. (eds.) Advances in Neural Information Processing Systems. vol. 32. Curran Associates, Inc. (2019)
25. Jacob, P., Éloi Zablocki, Ben-Younes, H., Chen, M., Pérez, P., Cord, M.: Steex: Steering counterfactual explanations with semantics (2021)
26. Jalwana, M.A.A.K., Akhtar, N., Bennamoun, M., Mian, A.: Cameras: Enhanced resolution and sanity preserving class activation mapping for image saliency. In: Proceedings of the IEEE/CVF Conference on Computer Vision and Pattern Recognition (CVPR). pp. 16327–16336 (June 2021)
27. Joshi, S., Koyejo, O., Kim, B., Ghosh, J.: xgems: Generating exemplars to explain black-box models. ArXiv [abs/1806.08867](https://arxiv.org/abs/1806.08867) (2018)
28. Kenny, E.M., Keane, M.T.: On generating plausible counterfactual and semi-factual explanations for deep learning. Proceedings of the AAAI Conference on Artificial Intelligence **35**(13), 11575–11585 (May 2021), <https://ojs.aaai.org/index.php/AAAI/article/view/17377>
29. Kim, B., Wattenberg, M., Gilmer, J., Cai, C., Wexler, J., Viegas, F., sayres, R.: Interpretability beyond feature attribution: Quantitative testing with concept activation vectors (TCAV). In: Dy, J., Krause, A. (eds.) Proceedings of the 35th International Conference on Machine Learning. Proceedings of Machine Learning Research, vol. 80, pp. 2668–2677. PMLR (10–15 Jul 2018)

30. Kingma, D.P., Welling, M.: Auto-Encoding Variational Bayes. In: 2nd International Conference on Learning Representations, ICLR 2014, Banff, AB, Canada, April 14-16, 2014, Conference Track Proceedings (2014)
31. Kong, Z., Ping, W.: On fast sampling of diffusion probabilistic models. In: ICML Workshop on Invertible Neural Networks, Normalizing Flows, and Explicit Likelihood Models (2021)
32. Kynkäänniemi, T., Karras, T., Laine, S., Lehtinen, J., Aila, T.: Improved precision and recall metric for assessing generative models. CoRR **abs/1904.06991** (2019)
33. Lee, J.R., Kim, S., Park, I., Eo, T., Hwang, D.: Relevance-cam: Your model already knows where to look. In: Proceedings of the IEEE/CVF Conference on Computer Vision and Pattern Recognition (CVPR). pp. 14944–14953 (June 2021)
34. Liu, S., Kailkhura, B., Loveland, D., Han, Y.: Generative counterfactual introspection for explainable deep learning. In: 2019 IEEE Global Conference on Signal and Information Processing (GlobalSIP). pp. 1–5 (2019)
35. Liu, Z., Luo, P., Wang, X., Tang, X.: Deep learning face attributes in the wild. In: Proceedings of International Conference on Computer Vision (ICCV) (December 2015)
36. Looveren, A.V., Klaise, J.: Interpretable counterfactual explanations guided by prototypes. In: Joint European Conference on Machine Learning and Knowledge Discovery in Databases. pp. 650–665. Springer (2021)
37. Madry, A., Makelov, A., Schmidt, L., Tsipras, D., Vladu, A.: Towards deep learning models resistant to adversarial attacks. In: International Conference on Learning Representations (2018)
38. Meng, C., He, Y., Song, Y., Song, J., Wu, J., Zhu, J.Y., Ermon, S.: SDEdit: Guided image synthesis and editing with stochastic differential equations. In: International Conference on Learning Representations (2022)
39. Mothilal, R.K., Sharma, A., Tan, C.: Explaining machine learning classifiers through diverse counterfactual explanations. Proceedings of the 2020 Conference on Fairness, Accountability, and Transparency (2020)
40. Nauta, M., van Bree, R., Seifert, C.: Neural prototype trees for interpretable fine-grained image recognition. In: Proceedings of the IEEE/CVF Conference on Computer Vision and Pattern Recognition (CVPR). pp. 14933–14943 (June 2021)
41. Nemirovsky, D., Thiebaut, N., Xu, Y., Gupta, A.: CounterGAN: Generating realistic counterfactuals with residual generative adversarial nets. arXiv preprint arXiv:2009.05199 (2020)
42. Nichol, A.Q., Dhariwal, P.: Improved denoising diffusion probabilistic models (2021)
43. Park, D.H., Hendricks, L.A., Akata, Z., Rohrbach, A., Schiele, B., Darrell, T., Rohrbach, M.: Multimodal explanations: Justifying decisions and pointing to the evidence. In: Proceedings of the IEEE Conference on Computer Vision and Pattern Recognition (CVPR) (June 2018)
44. Pawelczyk, M., Agarwal, C., Joshi, S., Upadhyay, S., Lakkaraju, H.: Exploring Counterfactual Explanations Through the Lens of Adversarial Examples: A Theoretical and Empirical Analysis. arXiv:2106.09992 [cs] (Jun 2021)
45. Petsiuk, V., Das, A., Saenko, K.: RISE: randomized input sampling for explanation of black-box models. In: British Machine Vision Conference 2018, BMVC 2018, Newcastle, UK, September 3-6, 2018. p. 151. BMVA Press (2018)
46. Petsiuk, V., Jain, R., Manjunatha, V., Morariu, V.I., Mehra, A., Ordonez, V., Saenko, K.: Black-box explanation of object detectors via saliency maps. In: IEEE Conference on Computer Vision and Pattern Recognition, CVPR 2021, virtual, June 19-25, 2021. pp. 11443–11452. Computer Vision Foundation / IEEE (2021)

47. Poyiadzi, R., Sokol, K., Santos-Rodríguez, R., Bie, T.D., Flach, P.A.: Face: Feasible and actionable counterfactual explanations. Proceedings of the AAAI/ACM Conference on AI, Ethics, and Society (2020)
48. Rodríguez, P., Caccia, M., Lacoste, A., Zamparo, L., Laradji, I., Charlin, L., Vazquez, D.: Beyond trivial counterfactual explanations with diverse valuable explanations. In: Proceedings of the IEEE/CVF International Conference on Computer Vision (ICCV). pp. 1056–1065 (October 2021)
49. Saharia, C., Chan, W., Chang, H., Lee, C.A., Ho, J., Salimans, T., Fleet, D.J., Norouzi, M.: Palette: Image-to-image diffusion models. In: NeurIPS 2021 Workshop on Deep Generative Models and Downstream Applications (2021)
50. Saharia, C., Ho, J., Chan, W., Salimans, T., Fleet, D., Norouzi, M.: Image super-resolution via iterative refinement. ArXiv **abs/2104.07636** (2021)
51. Sauer, A., Geiger, A.: Counterfactual generative networks. In: 9th International Conference on Learning Representations, ICLR 2021, Virtual Event, Austria, May 3-7, 2021. OpenReview.net (2021)
52. Schut, L., Key, O., Mc Grath, R., Costabello, L., Sacaleanu, B., Corcoran, M., Gal, Y.: Generating interpretable counterfactual explanations by implicit minimisation of epistemic and aleatoric uncertainties. In: Banerjee, A., Fukumizu, K. (eds.) Proceedings of The 24th International Conference on Artificial Intelligence and Statistics. Proceedings of Machine Learning Research, vol. 130, pp. 1756–1764. PMLR (13–15 Apr 2021)
53. Selvaraju, R.R., Cogswell, M., Das, A., Vedantam, R., Parikh, D., Batra, D.: Grad-cam: Visual explanations from deep networks via gradient-based localization. In: Proceedings of the IEEE International Conference on Computer Vision (ICCV) (Oct 2017)
54. Shih, S.M., Tien, P.J., Karnin, Z.: GANMEX: One-vs-one attributions using GAN-based model explainability. In: Meila, M., Zhang, T. (eds.) Proceedings of the 38th International Conference on Machine Learning, ICML 2021, 18-24 July 2021, Virtual Event. Proceedings of Machine Learning Research, vol. 139, pp. 9592–9602. PMLR (2021)
55. Singla, S., Pollack, B., Chen, J., Batmanghelich, K.: Explanation by progressive exaggeration. In: International Conference on Learning Representations (2020)
56. Song, J., Meng, C., Ermon, S.: Denoising diffusion implicit models. In: International Conference on Learning Representations (2021)
57. Song, Y., Sohl-Dickstein, J., Kingma, D.P., Kumar, A., Ermon, S., Poole, B.: Score-based generative modeling through stochastic differential equations. In: International Conference on Learning Representations (2021)
58. Tan, S., Caruana, R., Hooker, G., Koch, P., Gordo, A.: Learning global additive explanations for neural nets using model distillation (2018)
59. Thiagarajan, J.J., Narayanaswamy, V., Rajan, D., Liang, J., Chaudhari, A., Spanias, A.: Designing counterfactual generators using deep model inversion. In: Beygelzimer, A., Dauphin, Y., Liang, P., Vaughan, J.W. (eds.) Advances in Neural Information Processing Systems (2021), <https://openreview.net/forum?id=iHisgL7PFj2>
60. Van Looveren, A., Klaise, J., Vacanti, G., Cobb, O.: Conditional generative models for counterfactual explanations. arXiv preprint arXiv:2101.10123 (2021)
61. Vandenhende, S., Mahajan, D., Radenovic, F., Ghadiyaram, D.: Making heads or tails: Towards semantically consistent visual counterfactuals. arXiv preprint arXiv:2203.12892 (2022)

62. Vasu, B., Long, C.: Iterative and adaptive sampling with spatial attention for black-box model explanations. In: Proceedings of the IEEE/CVF Winter Conference on Applications of Computer Vision (WACV) (March 2020)
63. Wachter, S., Mittelstadt, B., Russell, C.: Counterfactual Explanations Without Opening the Black Box: Automated Decisions and the GDPR. *arXiv Journal of Law and Technology*, **31**(2), 841–887 (2018). <https://doi.org/10.2139/ssrn.3063289>
64. Wang, H., Wang, Z., Du, M., Yang, F., Zhang, Z., Ding, S., Mardziel, P., Hu, X.: Score-cam: Score-weighted visual explanations for convolutional neural networks. In: Proceedings of the IEEE/CVF Conference on Computer Vision and Pattern Recognition (CVPR) Workshops (June 2020)
65. Wang, P., Li, Y., Singh, K.K., Lu, J., Vasconcelos, N.: Imagine: Image synthesis by image-guided model inversion. In: Proceedings of the IEEE/CVF Conference on Computer Vision and Pattern Recognition (CVPR). pp. 3681–3690 (June 2021)
66. Wang, P., Vasconcelos, N.: Scout: Self-aware discriminant counterfactual explanations. In: Proceedings of the IEEE/CVF Conference on Computer Vision and Pattern Recognition. pp. 8981–8990 (2020)
67. Watson, D., Ho, J., Norouzi, M., Chan, W.: Learning to efficiently sample from diffusion probabilistic models. *CoRR* **abs/2106.03802** (2021)
68. Xian, Y., Sharma, S., Schiele, B., Akata, Z.: F-vaegan-d2: A feature generating framework for any-shot learning. In: Proceedings of the IEEE/CVF Conference on Computer Vision and Pattern Recognition (CVPR) (June 2019)
69. Yeh, C.K., Kim, B., Arik, S.Ö., Li, C.L., Pfister, T., Ravikumar, P.: On completeness-aware concept-based explanations in deep neural networks. *arXiv: Learning* (2020)
70. Yuhki Hatakeyama, Hiroki Sakuma, Y.K., Suenaga, K.: Visualizing color-wise saliency of black-box image classification models. In: Asian Conference on Computer Vision (ACCV) (2020)
71. Zhang, Q., Wu, Y.N., Zhu, S.C.: Interpretable convolutional neural networks. In: Proceedings of the IEEE Conference on Computer Vision and Pattern Recognition (CVPR) (June 2018)
72. Zhang, R., Isola, P., Efros, A.A., Shechtman, E., Wang, O.: The unreasonable effectiveness of deep features as a perceptual metric. In: Proceedings of the IEEE Conference on Computer Vision and Pattern Recognition (CVPR) (June 2018)
73. Zhao, Z., Dua, D., Singh, S.: Generating natural adversarial examples. In: 6th International Conference on Learning Representations, ICLR 2018, Vancouver, BC, Canada, April 30 - May 3, 2018, Conference Track Proceedings. OpenReview.net (2018)
74. Zhou, B., Khosla, A., Lapedriza, A., Oliva, A., Torralba, A.: Learning deep features for discriminative localization. In: Proceedings of the IEEE Conference on Computer Vision and Pattern Recognition (CVPR) (June 2016)
75. Zhou, B., Sun, Y., Bau, D., Torralba, A.: Interpretable basis decomposition for visual explanation. In: Proceedings of the European Conference on Computer Vision (ECCV) (September 2018)